

Article

Modelling and Mapping Total and Bioaccessible Arsenic and Lead in Stoke-on-Trent and Their Relationships with Industry

Joanna Wragg *  and Mark Cave 

British Geological Survey, Keyworth, Nottingham NG12 5GG, UK; mrca@bgs.ac.uk

* Correspondence: jwrag@bgs.ac.uk

Abstract: This study was based on a geochemical soil survey of Stoke-on-Trent in the UK of 747 surface soil samples analysed for 53 elements. A subset of 50 of these soil samples were analysed for their bioaccessible As and Pb content using the Unified Barge Method. Random Forest modelling, using the total element data as predictor variables, was used to predict bioaccessible As and Pb for all 747 samples. Random Forest modelling, using inverse distance weighed predictors and bedrock and superficial geology, was also used to map both total and bioaccessible As and Pb on a 400 × 400 spatial prediction grid with a 50 m resolution. The predicted bioaccessible As ranged from ca. 1 to 8 mg/kg and the total As ca. 8 to 45 mg/kg. The bioaccessible Pb and the total Pb both covered the range ca. 16–1200 mg/kg, with the highest values for both forms of Pb showing similar spatial distributions. Predictor variable importance and information on past industry suggest that the source of both of these elements is driven by anthropogenic causes.

Keywords: arsenic; lead; soil; Stoke-on-Trent; bioaccessibility



Citation: Wragg, J.; Cave, M. Modelling and Mapping Total and Bioaccessible Arsenic and Lead in Stoke-on-Trent and Their Relationships with Industry. *Geosciences* **2021**, *11*, 515. <https://doi.org/10.3390/geosciences11120515>

Academic Editors: Javier Lillo and Jesus Martinez-Frias

Received: 8 November 2021

Accepted: 13 December 2021

Published: 15 December 2021

Publisher's Note: MDPI stays neutral with regard to jurisdictional claims in published maps and institutional affiliations.



Copyright: © 2021 by the authors. Licensee MDPI, Basel, Switzerland. This article is an open access article distributed under the terms and conditions of the Creative Commons Attribution (CC BY) license (<https://creativecommons.org/licenses/by/4.0/>).

1. Introduction

Soils act as sinks and sources of potentially harmful elements (PHE), which can be associated with the underlying geology and deposition of contaminants from previous land use. The range and distribution of past and present industrial activity provides a challenge for understanding the complex mixtures of contaminants in soils. The potential hazard to human health from reuse of this land (e.g., housing and greenspace) can be assessed by the identification and quantification of the total soil PHE content, but this can overestimate the potential hazard to human health, as it assumes that the total content will be available for uptake in the human body after accidental exposure [1,2]. To reflect solubility of soil PHE after accidental exposure, bioaccessible studies provide a physicochemical estimation of the amount of contaminant available for uptake in the body. Understanding the sources of PHE and, as a result, the potential mobility is therefore important in efforts to understand the potential for—and impacts of—repurposing of land.

Stoke-on-Trent is a post-industrial city in North Staffordshire, UK. The city, an amalgam of six towns (Burslem, Longton, Stoke, Tunstall, Fenton and Hanley), covers an area of 36 square miles (93 km²) and has a combined population of ca. 250,000 (Figure 1) [3]. Known as the ‘potteries’, Stoke was the home of the pottery industry in England, with over 100 potteries between the 1700s and the present day [4,5]. Many of these were owned by different generations of the same families and, with others, amalgamated over time. Notable pottery manufacturers include Royal Doulton, Middleport and Wedgewood in Burslem, Dresden and Gladstone in Longton and Spode and Minton in Stoke [5]. In addition to tableware potteries, there were sanitary ware manufacturers, such as Armitage Shanks and Twyfords. The pottery industry was initially founded on the abundance of coal and clay suitable for earthenware and brick production (e.g., Grey and Etruria Marls, Fireclays) which overlay the Coal Measures [6,7]. Later, the importation of China clay supported the development of more delicate tableware.

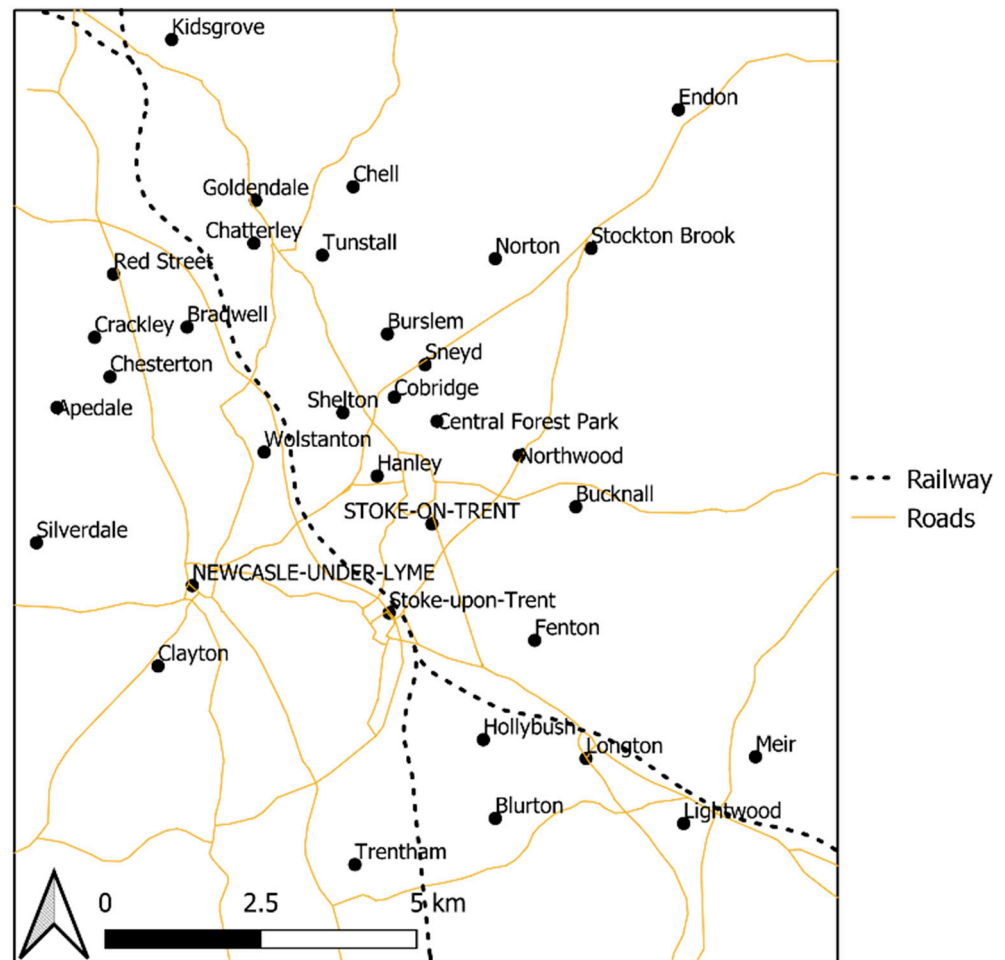


Figure 1. Map of Stoke-on-Trent and surrounding towns.

Manufacture of colours and chemicals for potteries, glazed bricks manufacturers, glassmakers and enamellers were also present across the area. The variety and colour of pottery was derived from the metal oxides (Cd, Cr, Cu, Co, Fe, Mn, Ni, U and V) and the composition of the glazes (SiO_2 , Al_2O_3 , CaO, SnO_2 PbO and FeTiO_2) used in the decorative processes [8].

The Staffordshire coalfield supported the development of Stoke as an industrial city. Stretching from Madely in the west, the coalfields went as far as the Towerhill colliery in the north and the Foxfield and Hem Heath collieries in the east and south, respectively [9]. Early workings of the coal measures were established around the Hanley, Burslem, Tunstall and Longton areas of the city, with deep pits at Chatterley, Whitfield and the Red Street area central to opencast mining. Naturally elevated concentrations of PHE, such as As, V, Mo, Cu, Ni, Zn, Pb, can be found in the coal measures that surround the city [8].

Stoke-on-Trent was also home to numerous steel and iron works. The largest of these was the Shelton Bar Steelworks, which stretched across the Etruria Valley. The works, at its height, employed a workforce of 10,000 and included multiple coal mines, steelworks, rolling mills and blast furnaces before finally closing in 2000. To reduce the distance between the fuel and the furnace, furnaces would be on the same site as the coal mine.

Industrial activity in Stoke, including provision of raw materials for both the pottery and steel industries (and exportation of products), was supported by multiple transport links. Railway lines running through the city included what is now known as the West Coast Mainline (WCM) and the North Staffordshire Railway (NSR). Tramways and mineral railway lines crossed the region, providing vital links between the coalfields and claypits and the potteries and local industries. One such linkage was the potteries' loop line [10].

The loop line ran from the Etruria works to Kidsgrove. Additional support was provided through the construction of the Trent/Mersey and Cauldon canals, which ran alongside the WCM and NSR, respectively. Engineering, carriage and wagon works were situated in the area to support rail activity.

The rapid growth of the local pottery and steel industries (and the large supporting coal industry) resulted in a large conurbation mixing residential, retail and industrial developments. The by-products of the range of activities in Stoke included furnace slag and ceramic waste, which were often repurposed as sources of urban fill and made into ground material for the building of required urban infrastructure as the city grew [8].

The industry of Stoke has left a landscape rich in industrial heritage, as shown in Figure 2, characterised by the once widespread bottle kilns, canals, wharfages and dis-used railways. Regeneration of Stoke has repurposed large areas of previously used and potentially contaminated land for industrial, residential and community/greenspace use (Figure 3, Table 1) today, over one third of the city is green, open space [11].

In this work, we chose to study the total bioaccessible concentrations and spatial distribution of As and Pb, common priority soil contaminants, for human health risk assessment. The work used modelling approaches to identify PHE relationships to naturally occurring and anthropogenic elements from historical land use found concurrently in soil samples for the development of predictive distribution maps to support future urban planning activities.

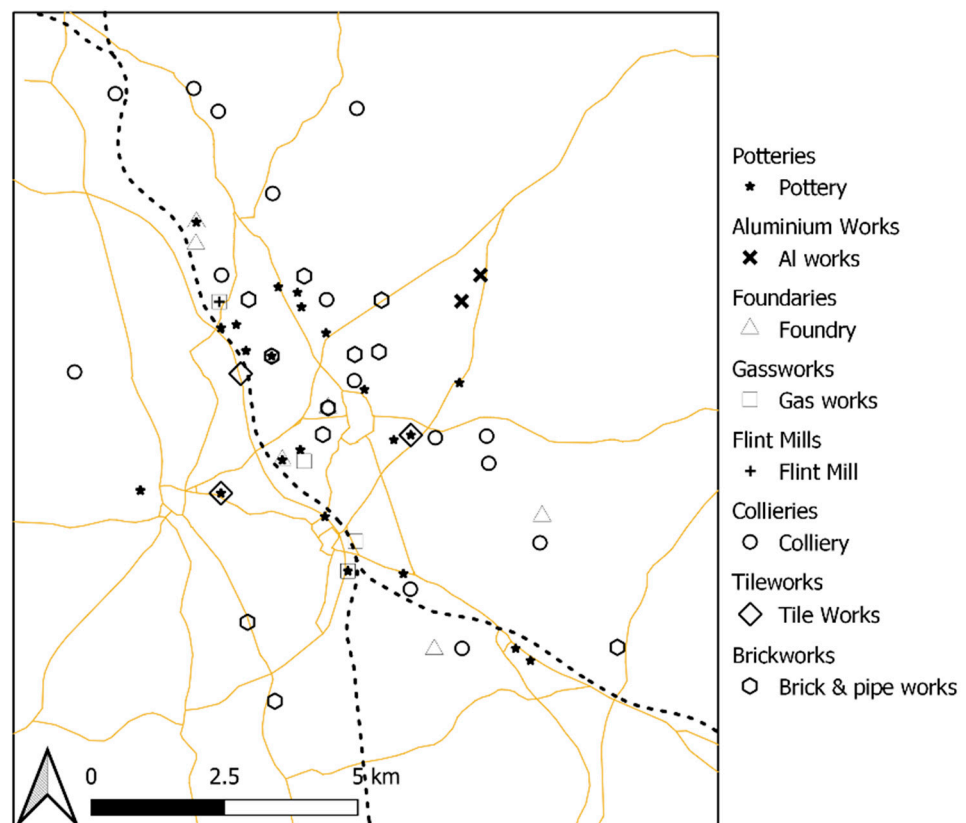


Figure 2. Location of selected industrial sites in Stoke-on-Trent.

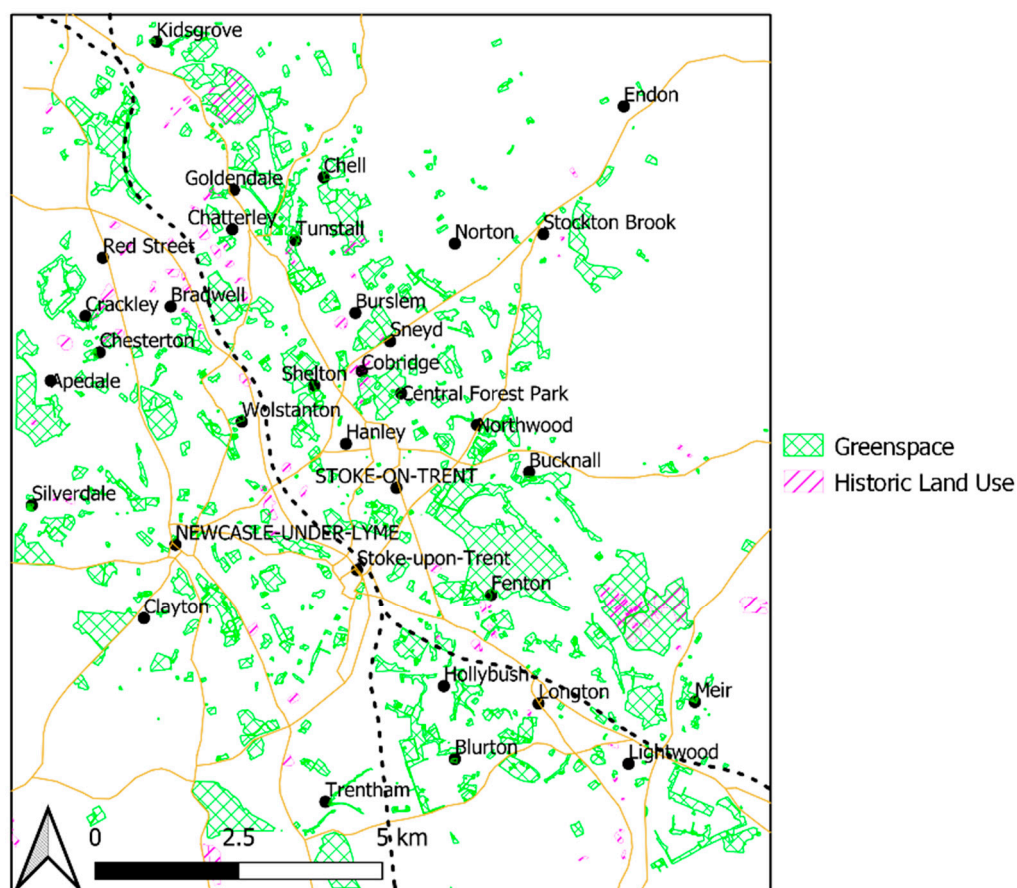


Figure 3. Greenspace development of industrial sites.

Table 1. Regeneration of Industrial sites.

Location/Land Use	Land Use Post Regeneration
Apedale Mine/Ironworks	Country Park
Birchenwood Colliery Tip	Industrial Estate
Chatterley Whitfield	Parkland
Chell Railway Cutting Colliery infill	Parkland
Chell Quarry	Athletic Stadium
Cobridge Clay Pit	Industrial Estate
Etruria, Festival Park	Country Park
Fenton Colliery Tip	Industrial Estate
Lightwood Quarry	Housing Estate
Parkhouse Colliery Tip	Industrial Estate
Red Street Opencast Mine	Housing
Rowhurst Clay Pit	Industrial Estate
Silverdale Colliery Tip	Pasture/Country Park
Shelton Colliery Tip/Ironworks	Industrial Estate
Sneyd Hill	Community Land
Tunstall Clay Pit	Industrial Estate

2. Materials and Methods

2.1. Soil Sampling and Analysis

The soil samples were part of the British Geological Survey (BGS) Geochemical Survey of Urban Environments (GSUE) project [8], an integral part of the wider G-BASE and TellusNI programmes. The aim of the programme was to provide an overview of the geochemical signature of urban environments. Four samples were collected from within each national grid—one km square on 1:25,000 topographic Ordnance Survey map. Each was collected from the least disturbed area of unbuilt ground as close as possible to the centre of 500 m sub-cells. Areas sampled included domestic gardens, allotments, parks, recreational ground, or road verges, avoiding point sources of contamination. The surface soils ($n = 747$), collected in 1993, were sampled at a depth of 0.15 m using a handheld auger, air-dried and sieved to <2 mm. Fordyce et al. [8] described the details of the sampling procedures and soil preparation as well as analytical details for the measurement of total element concentrations by X-Ray fluorescence (XRF).

Bioaccessibility measurements (As and Pb) were carried out on a subset of 50 of the 747 soil samples collected. In order to ensure that the 50 samples were representative of the overall data set, the soil geochemical data was clustered according to elemental groupings. The geochemistry dataset was mean-centered and scaled to unit variance and clustered using the “mclust” model-based clustering algorithm based on parameterized finite Gaussian mixture models [12] within the R programming language [13]. Four clusters were identified as being a parsimonious representation of different variations in geochemistry over the region. They also represented the underlying geology. Between 10 and 17 samples were randomly chosen from each group to make up 50 samples.

The <2 mm soil samples were further sieved to <250 μm for total and bioaccessible PHE determination. Total element (e.g., Al, As, Ba, Ca, Cd, Co, Cr, Cu, Fe, K, Mg, Mn, Mo, Na, Ni, P, Pb, Se, Si, Sr, V and Zn) concentrations in each sample were determined after mixed acid (HNO_3 , HF, HClO_4^-) digestion. The PHE bioaccessibility was measured after simulated gastrointestinal extraction using the Unified Barge Method (UBM). The UBM simulated the physicochemical conditions of the mouth, stomach and intestine by a 3-stage sequential extraction. Details of the background to the UBM and the procedure have been described in previous publications [14,15]. The total and bioaccessible concentrations were measured using Inductively Coupled Plasma-Mass Spectrometry as described in works by Middleton et al. [16] and Watts et al. [17].

For quality control purposes, one duplicate, one quality control soil (BGS 102) and one blank were extracted within every batch, at maximum, 10 unknown samples. Extraction data were in good agreement with the consensus values [18], with bioaccessible As and Pb concentrations for BGS 102 of 3.96 ± 0.12 mg/kg and 16.22 ± 1.62 mg/kg, respectively, and were also within the guidance values [18] and those reported by Hamilton et al., [19]. The repeatability (RSD) of both total and bioaccessible extraction duplicates was $<10\%$ RSD. All blank extractions (total and bioaccessible) returned values below the method detection limits.

2.2. Bioaccessibility Modelling

Bioaccessibility modelling, in this work, refers to the statistical analysis, data processing and quality assessment of actual measurements made in a subset of 50 representative samples for the production of reliable As and Pb bioaccessibility estimates for all 747 soil samples used in this study. Random Forest (RF) models for the bioaccessibility of As and Pb were set up using the UBM-measured bioaccessibility of the selected 50 samples as the dependent variable and a combination of the total element concentrations of 53 elements obtained by the G-BASE programme, with the sample elevations and the superficial and bedrock geology as possible predictor variables. The modelling was carried out using the R programming language [13] with the ranger library for RF modelling [20] and the Boruta library for selecting significant predictor variables [21]. The Boruta algorithm has been described in detail [21]; however, briefly: the Boruta Algorithm produces a duplicate predictor data set with each predictor randomly shuffled and joins the shuffled data set

with the original predictors. It then builds a random forest model on the merged dataset, making a comparison between the importance of the original variables with the randomised variables. Only variables having higher importance than the randomised variables are considered important.

The RF model set up for the two elements followed the procedure below:

1. Make an RF model for the bioaccessibility of the element in question using the ranger library.
2. Use the Boruta package to select out the significant predictors.
3. Optimise the new RF model r-square by varying the “mtry” parameter (the number of variables randomly sampled as candidates at each split) [20].
4. Run the optimised model 500 times, each time on a resampled dataset, predicting the bioaccessibility at all 747 sampling locations.
5. Take median and median absolute deviation (mad) values for the 500 predictions at each location to provide an estimate of the bioaccessibility and its associated modelled uncertainty at each location.

2.3. Spatial Modelling

Spatial modelling here refers to the statistical analysis, data processing and quality assessment procedures for the production of reliable estimates of As and Pb totals and bioaccessibility across a regular prediction grid of points covering the area of interest from 747 soil locations. Spatial modelling and prediction, for the purposes of illustrating the 2D distribution of a contaminant in soil, has traditionally been carried out using kriging-related techniques [22,23]. Recently, Hengl et al. [24] summarised the problems associated with kriging and demonstrated the use and advantages of a machine learning method (Random Forest, RF) for spatial modelling where buffer distances from observation points were used as explanatory variables. In other studies, Kirkwood et al. [25] used an RF model with high resolution geophysics and remote sensed data as covariates to produce a high resolution geochemical map of the South West of England. Additionally, Sekulić et al. [26] successfully demonstrated a similar RF approach using the nearest observations and their distances to the prediction location as covariates.

Random Forest (RF) is a popular machine learning algorithm that consists of an ensemble of randomised decision trees. Each tree is grown on a random subsample of the training data and a random subset of the predictor variables to choose from at each decision node. In this study, we used the RF modelling approach suggested by Cave [27], in which inverse distance weighted (IDW) covariates are used as the predictor variables and subsequently used to predict the spatial distribution of persistent organic pollutants in London [28]. Inverse distance weighted (IDW) interpolation explicitly makes the assumption that samples that are close to one another are more alike than those that are further apart [29]. To predict a value for any unmeasured location, IDW uses the measured values surrounding the prediction location. The measured values closest to the prediction location have more influence on the predicted value than those further away. IDW assumes that each measured point has a local influence that diminishes with distance. It gives greater weights to points closest to the prediction location, and the weights diminish as a function of distance—hence, the name inverse distance weighted [29]. IDW predictions require 2 parameters (the inverse distance power (p) and the number of nearest neighbours (n)) to use. While the premise behind IDW is broadly correct, the choice of p and n is subjective and there is no relation between the prediction and the actual spatial variability as in many other methods (e.g., in kriging, the model relates to the spatial variance of the parameter of interest through the variogram). In this instance, we took a series of IDW predictors with varying combinations of p and n and used these as the predictor covariates. Then, the RF model combined these covariates to model the estimated soil parameters at the prediction locations. The training set was produced by using leave-one-out (loo) IDW predictions for each sampled point and its associated contaminant concentration at each combination of p and n . IDW pseudo-predictions at the points where the predicted soil concentrations were

required were then calculated and used as predictor variables on the RF model produced on the training data.

The underlying geology of a region has been shown to be an important control on the geochemical composition of surface soils [30]. In addition to the IDW predictor covariates, the superficial geology and bedrock geology were used as predictor variables by attributing both the soil sample points and the prediction grid with the two geology variables.

2.3.1. Spatial Modelling Procedure

The data analysis was carried out using the R programming Language [13] and associated libraries. The “sf” R library [31] was used to attribute the geology data to the sampling points and prediction grid. The “ranger” R library [20] was used to carry out RF modelling. The Boruta R library [21] was used to select the significant predictor variables in the RF model. Preliminary checks (not reported) showed that, after the top 5–10 most important IDW predictor combinations, the inclusion of further IDW predictors did not meaningfully improve the root mean square error of prediction (RMSEP). The modelling and interpolation were carried out in the following stages:

1. A series of IDW predictor variables were made up from all combinations of nearest neighbour values of 3, 5, 7, 9, 11, 13, 15 and inverse distance power values of 0.1, 0.5, 0.9, 1.3, 1.7, 2.1, 2.5, 2.9 (56 combinations). For the training set, the IDW predictors were calculated for each individual point using a leave-one-out strategy. An RF model was set up using the 56 IDW combinations as predictor variables for the determinand in question.
2. The top 5 most important IDW combinations (measured in the RF model by the gini-index [17]) were chosen and combined with the geology data and used to produce a second RF model for the determinand in question. The second model was then subjected to the Boruta algorithm, which selected out the significant predictors (compared to randomly shuffled predictor variables [21]).
3. A third RF model using the significant geology and IDW predictors was then optimised to get the best value of “mtry” (the number of variables randomly sampled as candidates at each split in the decision trees used in the RF model [20]).
4. Finally, the third optimised RF model was applied to 100 bootstrap resamplings of the original sampling points (recalculating the IDW predictors for each bootstrap resample), with each of the resampling rounds producing data on the model fit and predictions for the determinand in question on the prediction grid. The final determinand prediction values at the prediction grid were calculated as the median value from the 100 resampling rounds.

2.3.2. Modelling Accuracy and Precision

Accuracy and precision [20] for the RF bioaccessibility modelling of As and Pb were assessed by comparing the so called “out of bag” (OOB) predicted values against the measured bioaccessible values for the selected 50 soil samples used to set up the model. The OOB data were, in effect, equivalent to cross-validated data (i.e., independent samples with measured values not used in setting up the model) because, within each of the RF model decision trees, bootstrapped samples of the original data were used so that the samples left out by the resampling could act as independent check samples.

A similar approach was used to estimate accuracy and precision [20] for the RF spatial modelling, this time using all 747 soil samples.

2.3.3. Selecting Significant Predictors

The Boruta algorithm [21] selects significant predictors by comparing their performance to a shadow set of predictors formed by randomly shuffling the original data. Through an iterative process, those parameters which perform better than the shadow predictors are selected as significant. The DALEX library in the R programming language [31] provides a method for post-analysing the RF model to derive the relative importance of the

predictor variables by measuring how much the root mean square error (RMSE) increases when a given parameter is randomly shuffled.

Similar approaches were used for both bioaccessibility and spatial modelling using 50 and 747 soil samples, respectively.

2.4. Relationship with Industry

The geochemistry maps were superimposed onto the Ordnance Survey New Popular Edition Historic map (1 inch to the mile) of Stoke-on-Trent (1940s) using QGIS [32] to visualise linkages between the industrial past and the spatial soil geochemistry of the area. This information, in conjunction with field notes taken at the time of sampling (e.g., waste material at the sampling locations) and information on the History of the County of Stafford [33] was used to identify previous land uses. Eight land uses were chosen for further discussion, but the sites referenced in this work were not a complete history of the activities, as a myriad of industries were prolific across the whole area. Table 2 provides an overview of land uses for the purposes of this work.

Table 2. Land use classifications.

Area	Dominant Industries
Tunstall (including Chell)	Potteries, coal and ironstone mining, foundry, AI works
Burslem (including Longport, Middleport and Cobridge)	Potteries, coal and ironstone mining, brickworks, gasworks, flint mill
Longton	Potteries, coal and ironstone mining, brickworks
Hanley (including Shelton and Etruria)	Potteries, foundry, flint mill, coal mining, brick and tileworks, gasworks
Stoke (including Boothen)	Potteries, gasworks
Fenton	Potteries, flint mill, coal and ironstone mining, brickwork and tileworks, locomotive works, foundry

3. Results

3.1. Bioaccessibility Modelling

The samples identified for bioaccessibility testing came from a variety of land uses, including industrial and railway sites, road junctions, housing estates and urban green spaces. The bioaccessible As concentration ranged between 0.66 and 11.4 mg/kg and bioaccessible Pb ranged from 5.77 to 413.9 mg/kg.

3.1.1. Arsenic Bioaccessibility

The fifty selected samples for bioaccessibility testing were originally analysed (<2 mm) for their total element content using XRF [8]. When the bioaccessibility of the <250 µm sub-samples was determined, the total As concentration was also measured by acid sample digestion and inductively-coupled plasma mass spectrometry (ICPMS). Figure 4A shows that there was good agreement between the XRF and ICPMS data, with the XRF As vs. ICPMS As lying close to the line of equivalence. Figure 4 also shows the observed linear relationship between the XRF total As and the stomach phase bioaccessible As (R-square = 0.54), with a slope suggesting that, on average, the bioaccessible As was ca. 21% of the total As.

The RF modelling accuracy and precision for the bioaccessible As, assessed from the OOB predicted values against the measured bioaccessible values for the selected 50 soil samples, are shown in (Figure 5). The distance of the points from the line of equivalence and the size of the vertical error bars on the OOB predictions provide the estimates for the accuracy and precision, respectively. The majority of the OOB-predicted values agreed with the actual values within the errors indicated by the error bars.

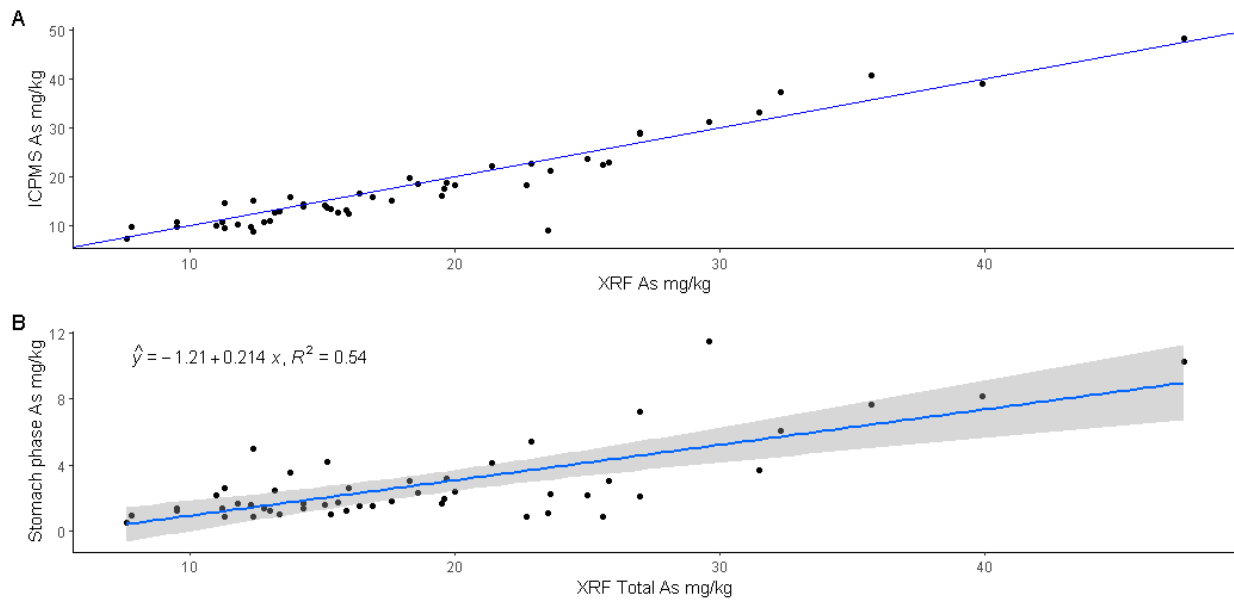


Figure 4. (A) Comparison of the XRF-determined total As with the ICPMS-determined As in 50 soil samples with line of equivalence. (B) Comparison of the XRF-determined total As with the bioaccessible stomach phase As in 50 soil samples with linear regression line and 90% confidence limit.

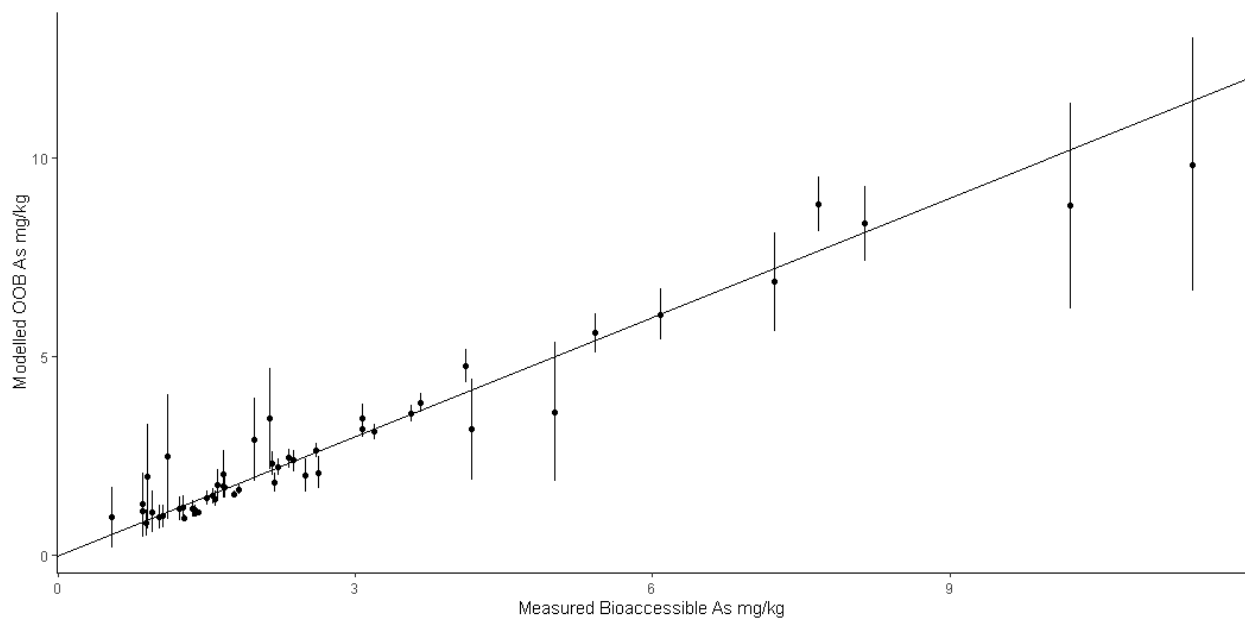


Figure 5. Accuracy and precision of the RF model for bioaccessible As. Straight line represents the line of equivalence and error bars are \pm the median absolute deviation.

The Boruta algorithm selects significant predictors by comparing their performance to a shadow set of predictors formed by randomly shuffling the original data. Through an iterative process, those parameters which perform better than the shadow predictors are selected as significant. The DALEX library in the R programming language [34] provides a method for post-analysing the RF model to derive the relative importance of the predictor variables by measuring how much the root mean square error increases when a given parameter is randomly shuffled. This measure of importance provides some insight on the geochemical factors controlling the bioaccessible As in the Stoke-on-Trent soils. Figure 6 shows that total Ca in the soil is the most important predictor, followed by the total As.

The sample elevations and the superficial and subsurface geology were not found to be significant predictor variables.

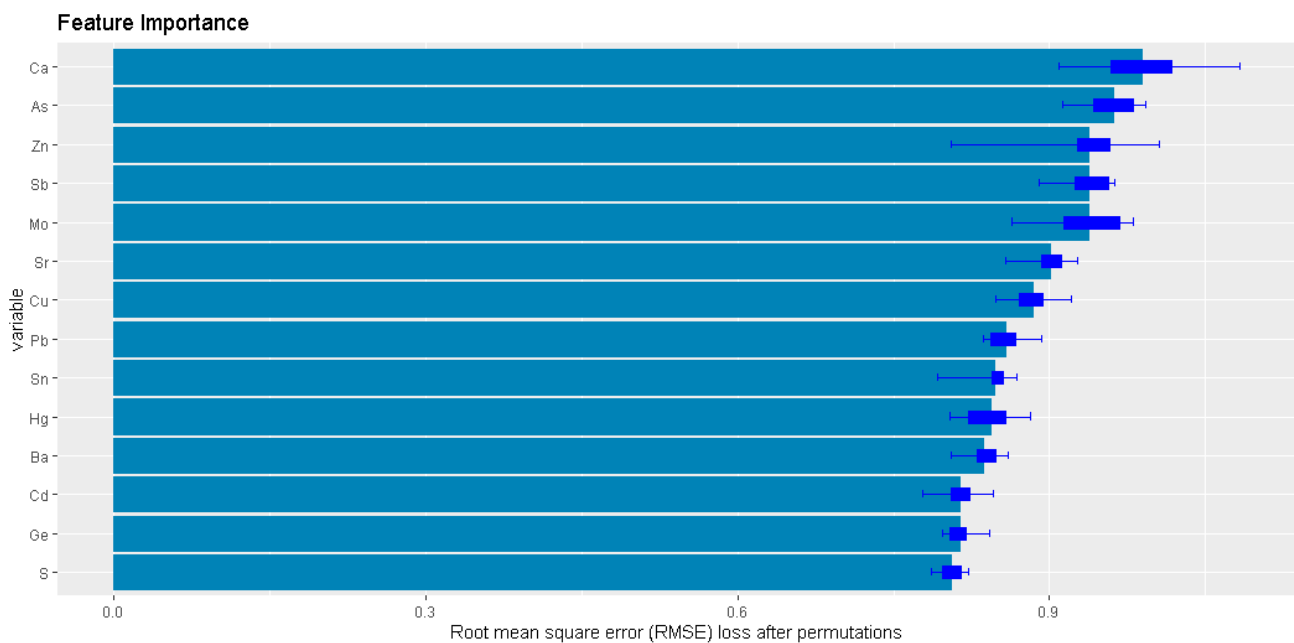


Figure 6. Relative importance of predictor variables for the RF model of the bioaccessible As.

This suggests that the bioaccessible As was associated with a carbonate phase in the soil. In addition, other significant predictors (such as Sb, Cu, Pb, Sn, Hg and Cd) are commonly associated with anthropogenic sources. This is in contrast with a study of Northampton [35] which is situated on underlying ironstone geology and where the bioaccessible As, measured using UBM, was associated with naturally-occurring fine-grained Fe oxyhydroxide in the soil. There, on average, the bioaccessible As was ca. 8% of the total As.

3.1.2. Lead Bioaccessibility

In a similar manner to the total As and bioaccessible measurements, Figure 7 shows that there was good agreement between the XRF and ICPMS data, with the XRF Pb vs. ICPMS Pb lying close to the line of equivalence. Figure 7 also shows that the relationship between the XRF total Pb and the stomach phase bioaccessible Pb was linear (R-square = 0.82), with a slope suggesting that, on average, the bioaccessible Pb was ca. 33% of the total Pb.

Figure 8 shows the accuracy and precision of the RF model for bioaccessible Pb. Figure 9 shows the relative importance of the significant predictor variables. In a similar manner to the As bioaccessibility, the sample elevations and the superficial and subsurface geology were not found to be significant predictor variables. In line with previous studies [36], Figure 9 shows that total Pb was the most significant predictor for bioaccessible Pb. However, the average bioaccessible Pb (as a fraction of total Pb) was towards the low end (ca. 33%, Figure 7B) compared to that previously reported (38% [36]) for the UK. In a more detailed study of Pb in the town of Northampton, it was suggested that the source of bioaccessible Pb in both rural and urban soils was a fine-grained pyromorphite mineral. In this instance, Figure 9 shows that the additional most important predictors (Hg, Ag, Sn) were more likely to be associated with industrial processes (e.g., Hg was used in gilded decoration on ceramics [37,38]) associated with the ceramics industry.

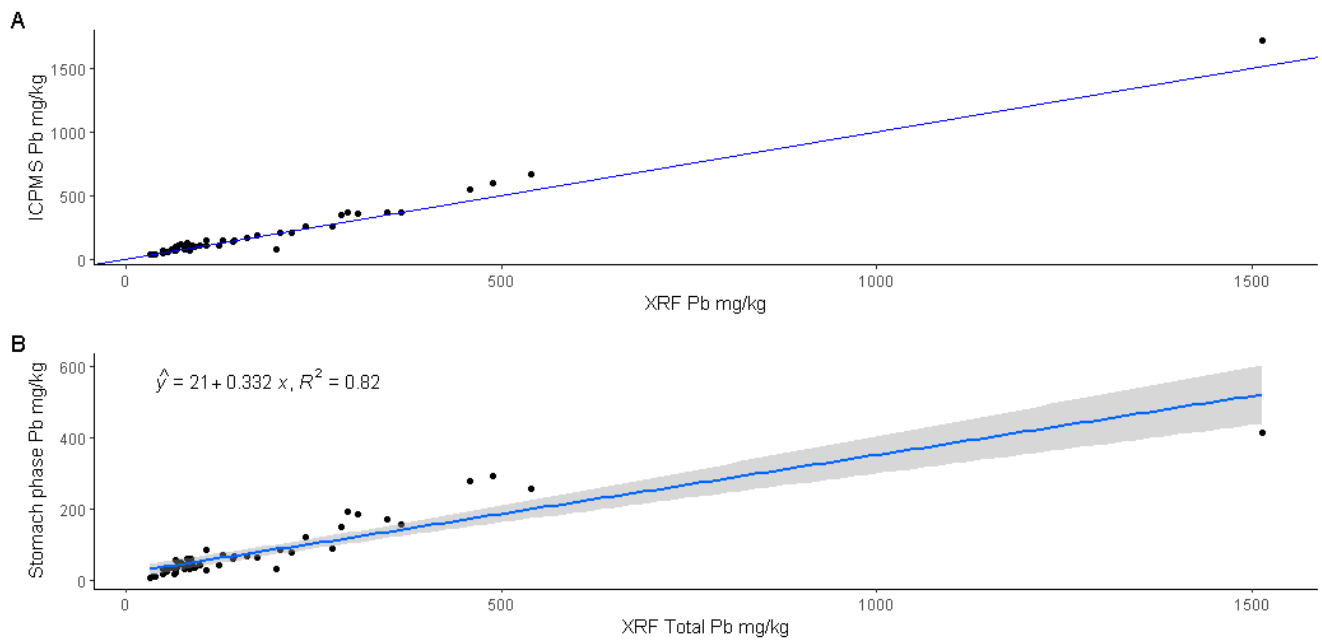


Figure 7. (A) Comparison of the XRF-determined total Pb with the ICPMS determined Pb in 50 soil samples with line of equivalence. (B) Comparison of the XRF-determined total Pb with the bioaccessible stomach phase Pb in 50 soil samples with linear regression line and 90% confidence limit.

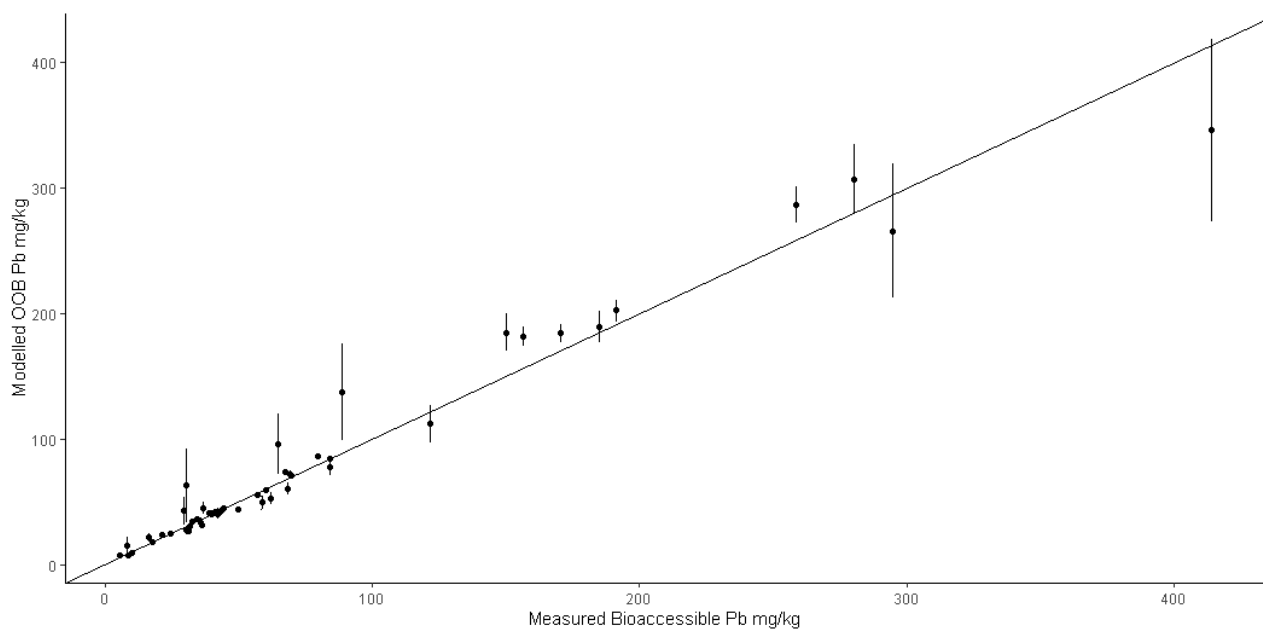


Figure 8. Accuracy and precision of the RF model for bioaccessible Pb. Straight line represents the line of equivalence and error bars are \pm the median absolute deviation.

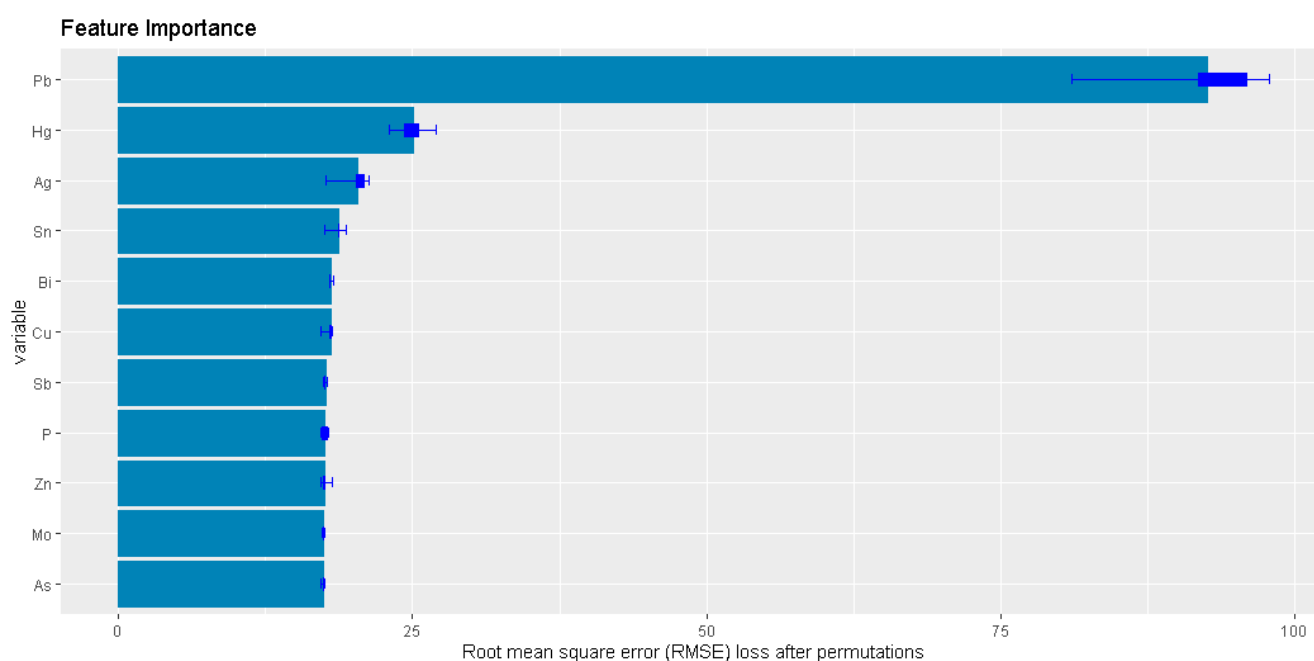


Figure 9. Relative importance of predictor variables for the RF model of the bioaccessible Pb.

3.2. Spatial Modelling of Total and Bioaccessible Concentrations

Spatial predictions of total As and total Pb and bioaccessible As and Pb were made over a 400×400 spatial prediction grid with a 50 m resolution which encompassed the soil sample locations. Table 3 gives the acronyms and the description of the bedrock and superficial geology that appear in various combinations as significant predictor variables for both As and Pb and their related bioaccessibility values.

Table 3. Significant geology predictor variables for the spatial modelling.

Formation Acronym	Formation Name	Formation Description	Formation Origin	Geology Type
HA	Halesowen formation	Sandstone	Sedimentary	Bedrock
CHES	Chester formation	Sandstone and conglomerate, interbedded	Sedimentary	Bedrock
ETM	Etruria formation	Sandstone	Sedimentary	Bedrock
PUCM	Pennine upper coal measures formation	Mudstone, siltstone and sandstone	Sedimentary	Bedrock
PMCM	Pennine middle coal measures formation	Mudstone, siltstone and sandstone	Sedimentary	Bedrock
ALV	Alluvium	Clay, silt, sand and gravel	Sedimentary	Superficial

In line with the RF bioaccessibility modelling, the performance and significant predictor variables for spatial modelling of total and bioaccessible As and Pb over the Stoke-on-Trent area were assessed by comparing the actual values with the OOB predictions and the significant variables. Additionally, we compared their relative importance using the Boruta algorithm [21] and DALEX post-processing of the optimized rf models [34].

In order to understand how the spatial predictions from the model were influenced by the predictor variables, *Ceteris-paribus* (Latin for “other things held constant”) profiles were constructed. These show how a model’s prediction will change if the value of a single exploratory variable is changed while keeping all other variables constant. By taking the averages of CP profiles for each of the training set samples for a given predictor variable, a partial dependence predictor profile for each variable was produced. This provided some insight into how that variable contributed to the overall model output.

Figure 10 shows the spatial extent of the each of the predictor geologies.

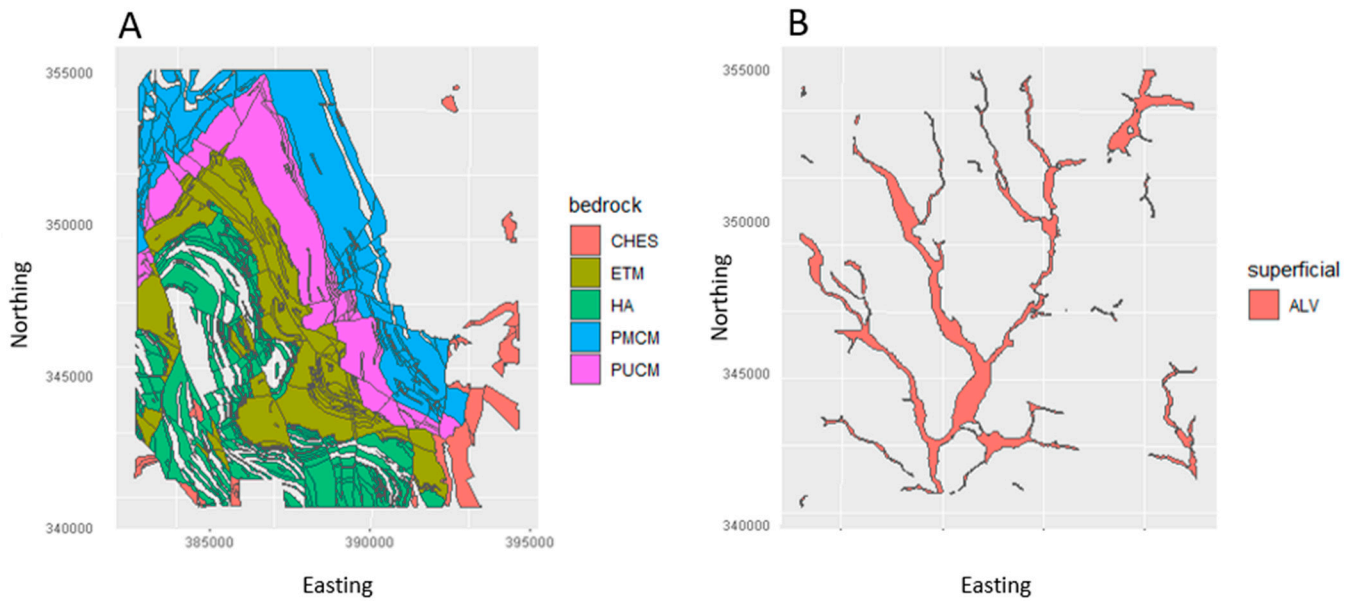


Figure 10. Significant bedrock (A) and superficial (B) geology predictors.

3.2.1. Arsenic

The accuracy and precision of the total and bioaccessible As values are shown in Figure 11. In both instances, apart from a few outliers, the majority of the OOB-predicted values agreed with the actual values within the errors indicated by the error bars. There was also some indication (Figure 11) that there was a small positive bias in both forms of As (total As > ca. 35 mg/kg and bioaccessible As > 5.5 mg/kg).

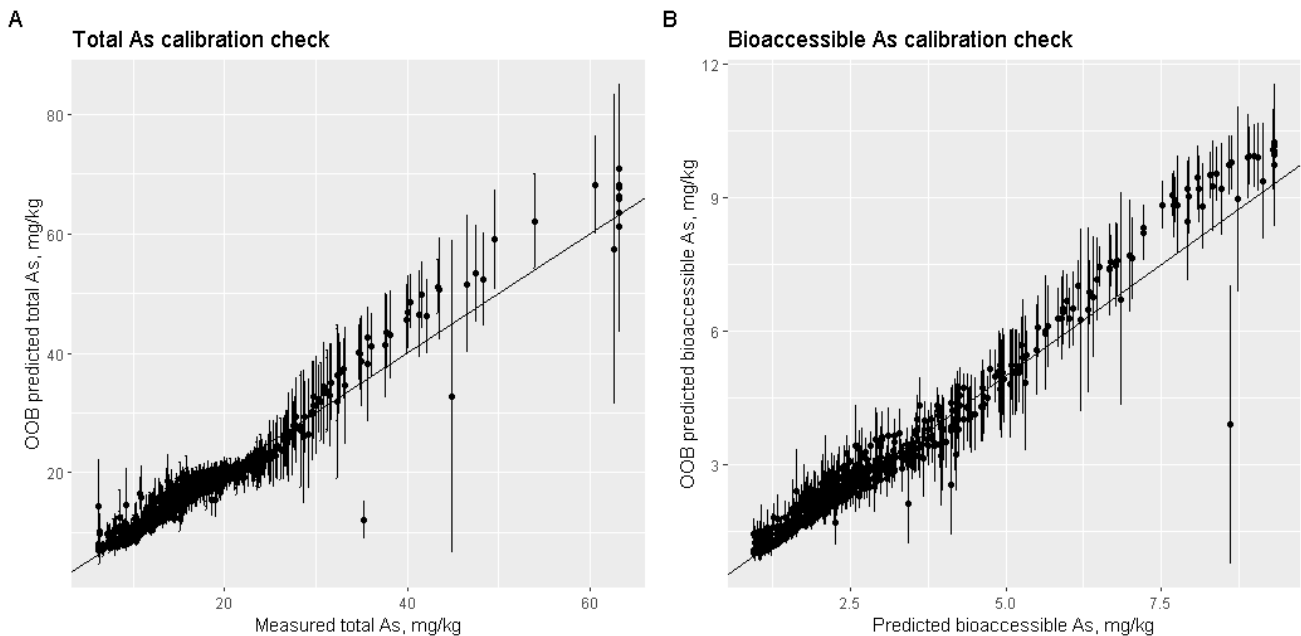


Figure 11. Calibration check for spatial predictions of total (A) and bioaccessible As (B). Solid line indicates the line of equivalence, points indicate the median predicted value and error bars are \pm the median absolute deviation.

Figure 12 shows the relative importance of the predictor variables for the spatial prediction of total and bioaccessible As and Figure 13 shows the partial dependence of these predictor variables. For total As predictions, geology predictor variables were more important than bioaccessible As (Figure 12), with higher total As in the Etruria formation (ETM) and Pennine middle coal measures formation (PMCM) and lower As in the Chester

formation (CHES) and Halesowen formation HA (Figure 13). For the bioaccessible As, the IDW variables were the most important predictor variables, with three geology predictors (ALV: Alluvium); PUCM: Pennine upper coal measures formation; PMCM: Pennine upper coal measures formation) found to be significant but still less important (Figure 12). With all three of these geological predictors, there was an increase in bioaccessible As in these formations (Figure 13). There was also a contrast in the shape of the partial dependence plots for the IDW predictors between the total and bioaccessible As (Figure 13). For the bioaccessible As, there was a relatively linear relationship between predicted values and the IDW prediction. Nevertheless, for total As, the relationship showed a relatively flat response, followed by a sharp increase at a breakpoint around IDW values of 20 mg/kg.

Whilst bioaccessible As was a subset of total As, the differences in the model predictors and the sensitivity of the prediction to the predictor variables suggested that the two forms of As derived from different sources, with total As being driven by natural abundance and anthropogenic sources and the bioaccessible fraction probably stemming from industrial influences (anthropogenic), as indicated by bioaccessibility modelling from the geochemistry data (Section 3.1.1).

Finally, the predicted total and bioaccessible As spatial prediction maps are shown in Figure 14 with the As concentrations split into deciles. The bioaccessible As ranged from ca. 1–8 mg/kg and the total As ranged from ca. 8–45 mg/kg. Figure 15 shows the bioaccessible fraction of As, where the highest values (16–57%) were concentrated in industrialized regions as indicated in Figures 2 and 3. This suggested once more that the bioaccessible As was associated with industrialized processes.

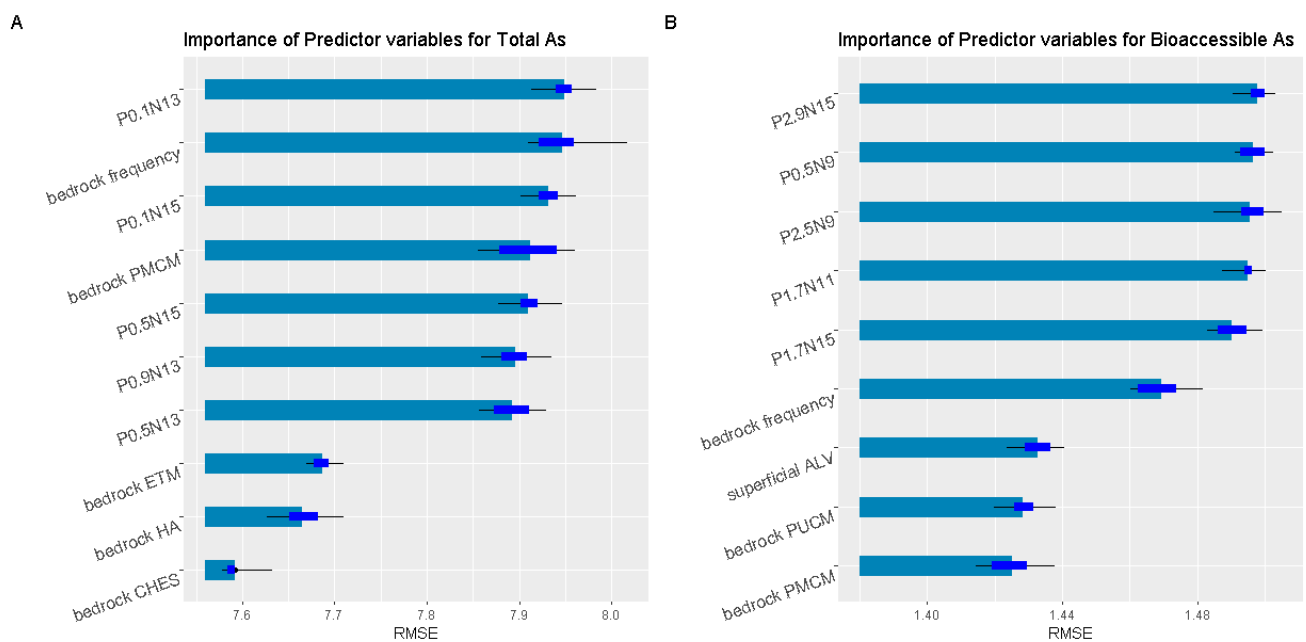


Figure 12. Relative importance of predictor variables for total (A) and bioaccessible As (B).

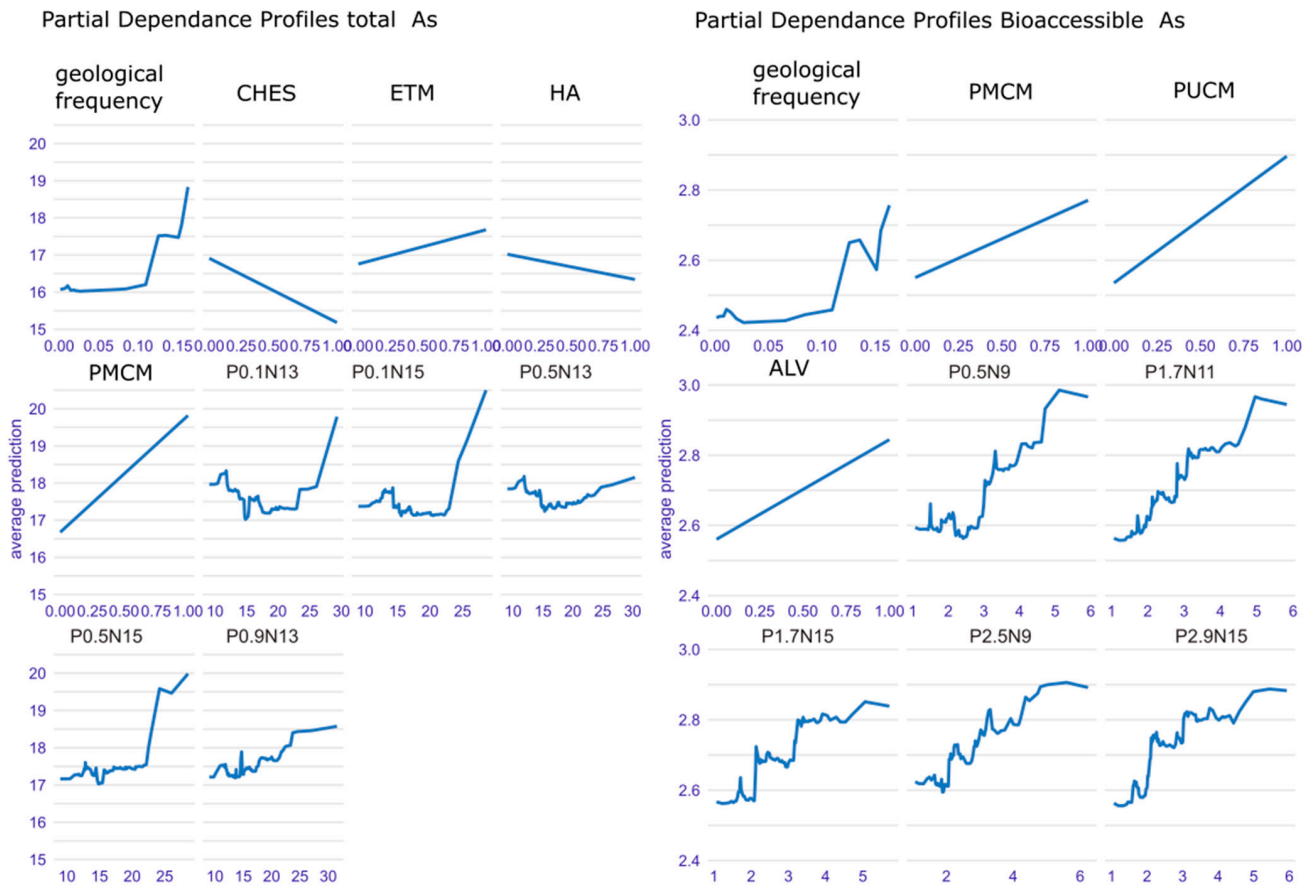


Figure 13. Partial dependence profiles for spatial prediction of total and bioaccessible As in soil.

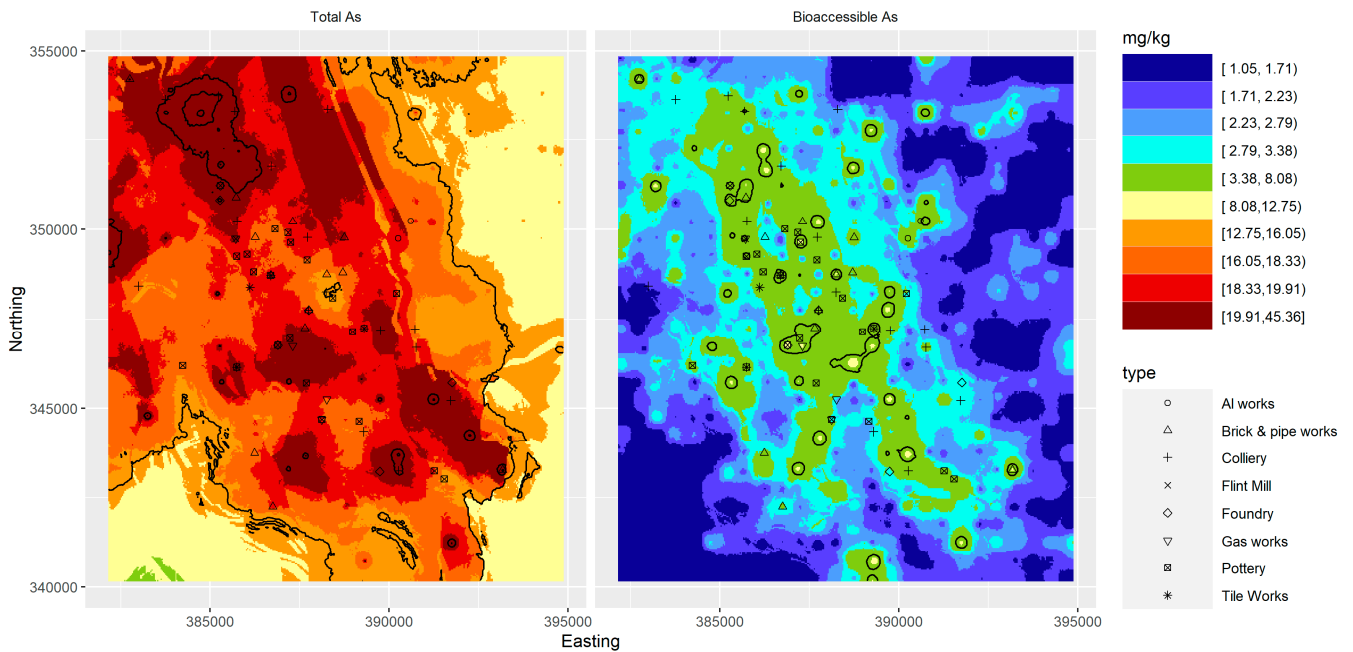


Figure 14. Spatial prediction of total and bioaccessible As in soil in Stoke-on-Trent along with locations of historic industry.

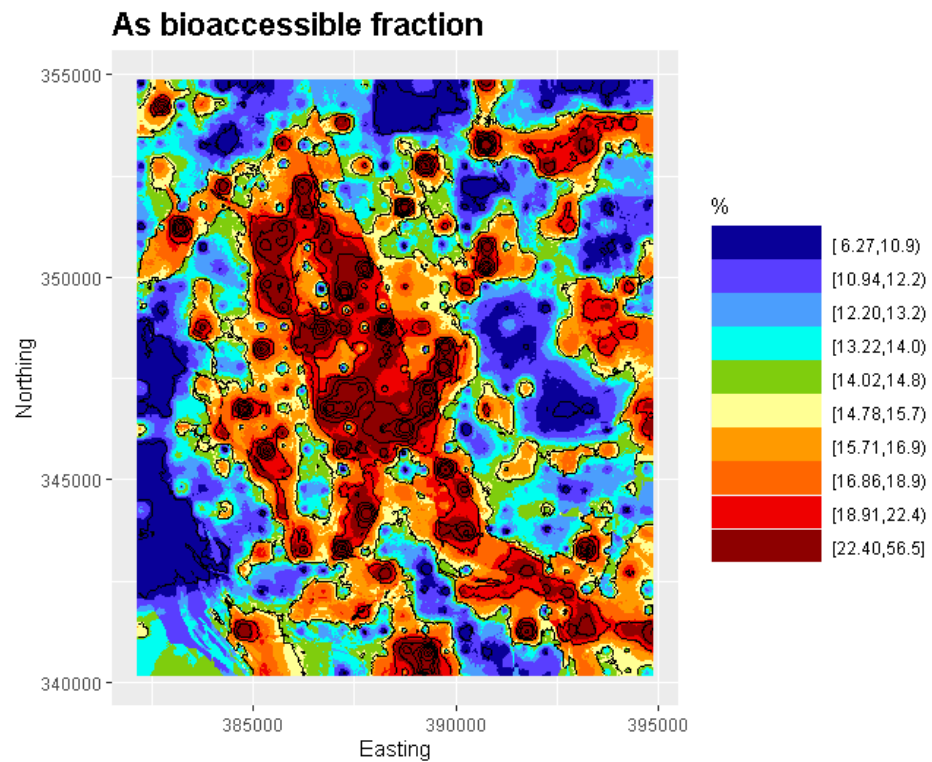


Figure 15. Bioaccessible fraction of As in soil in Stoke-on-Trent.

3.2.2. Lead

The accuracy and precision of the total and bioaccessible Pb are shown in Figure 16. For total Pb, apart from a few outliers, the majority of the OOB-predicted values agreed with the actual values within the errors indicated by the error bars. For bioaccessible Pb, the OOB-predicted values agreed with the actual values within errors, up to ca. 180 mg/kg. At higher values, there was some evidence of a positive bias (Figure 16).

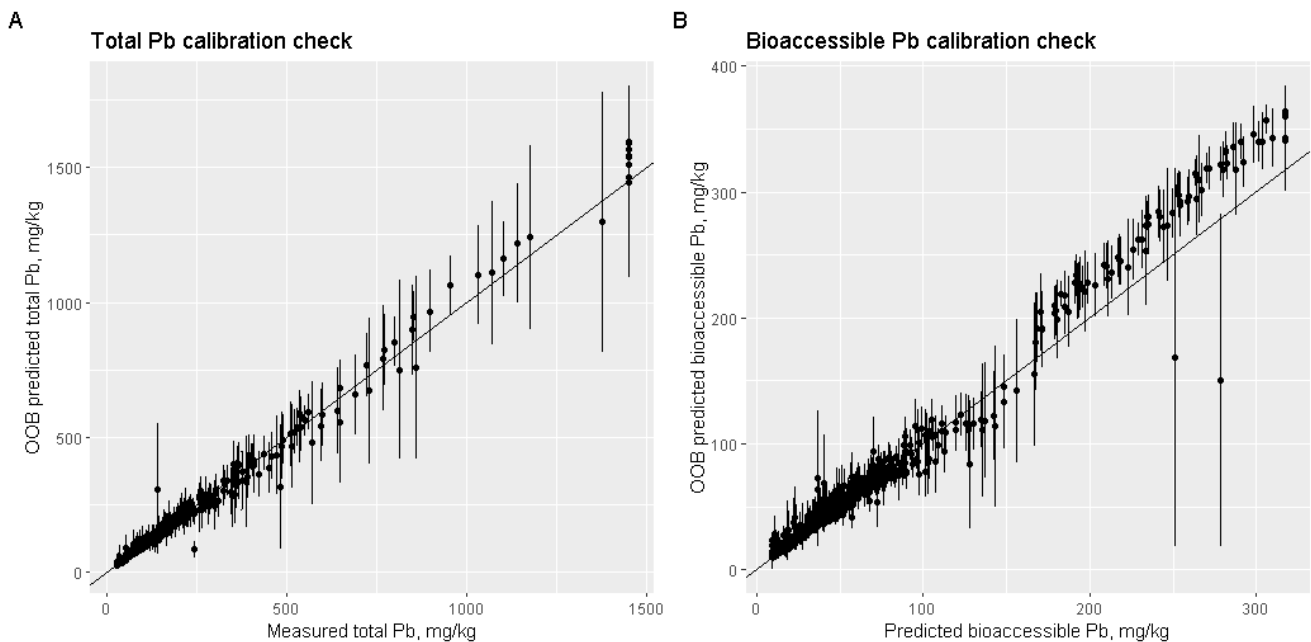


Figure 16. Calibration check for spatial predictions of total (A) and bioaccessible Pb (B). Solid line indicates the line of equivalence, points indicate the median predicted value and error bars are \pm the median absolute deviation.

Figure 17 shows the relative importance of the predictor variables for the spatial prediction of total and bioaccessible Pb and Figure 18 shows the partial dependence of these predictor variables. The IDW predictors were of the highest importance for both forms of Pb. There is an observably similar S shape for the partial dependence plots for the IDW predictors between the total and bioaccessible Pb (Figure 18). The similarity in the importance of predictor variables, the lack of importance of geological predictors, and the similarity of sensitivity to predictor variables (as shown by the partial dependence plots) suggested that both forms of lead were derived from a similar source (likely to be of industrial origin, as discussed in Section 3.1.2).

The predicted total and bioaccessible Pb spatial prediction maps are shown in Figure 19 with the Pb concentrations split into deciles. The bioaccessible Pb and total Pb both ranged from ca. 16–1234 mg/kg, with the highest values for both forms of Pb showing similar spatial distributions. Figure 20 shows the bioaccessible fraction of Pb which, in contrast to As, showed lower % bioaccessibility over the more industrialised areas, indicating that it was less environmentally mobile than As. The Pb bioaccessibility modelling (Section 3.1.2) suggested that bioaccessible Pb related to the glazes used in the ceramic industry were likely to be less mobile. The spatial distribution of the bioaccessible fraction could be explained by higher concentrations of the this less mobile form in areas related to ceramics production.

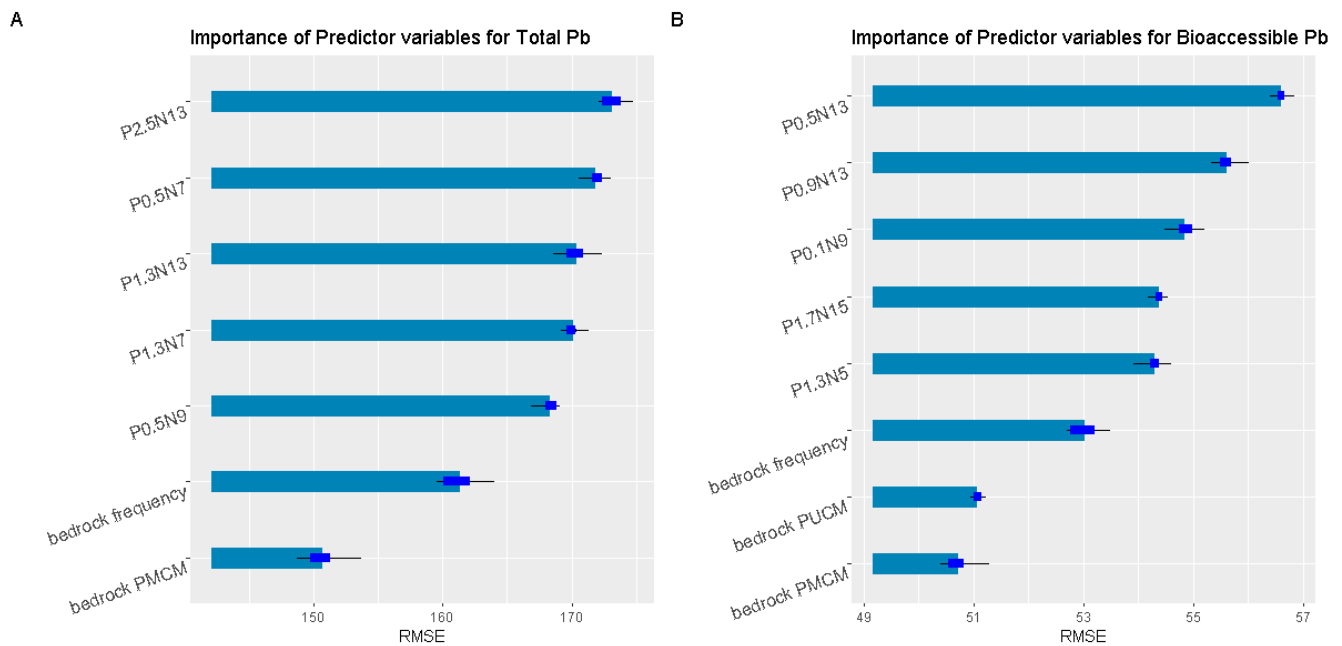


Figure 17. Relative importance of predictor variables for total (A) and bioaccessible Pb (B).

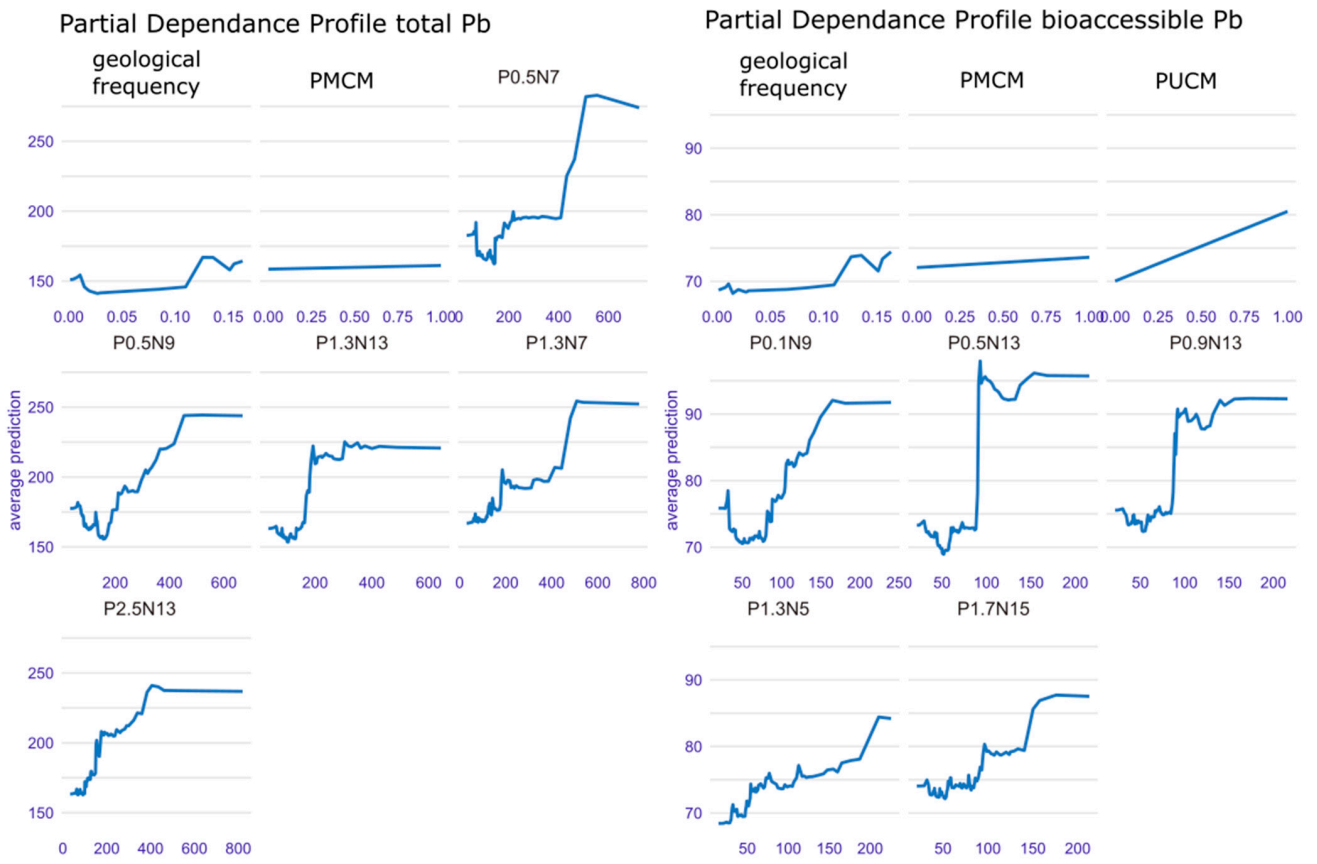


Figure 18. Partial dependence profiles for spatial prediction of total and bioaccessible Pb in soil.

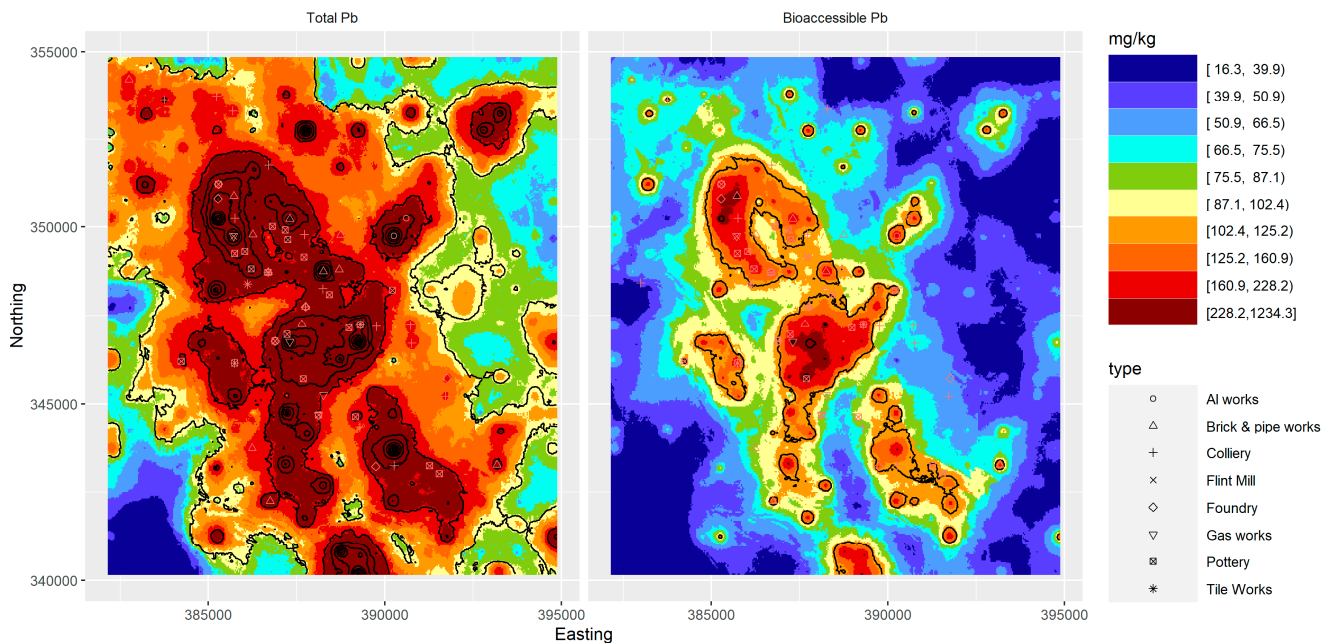


Figure 19. Spatial prediction of total and bioaccessible Pb in soil in Stoke-on-Trent along with locations of historic industry.

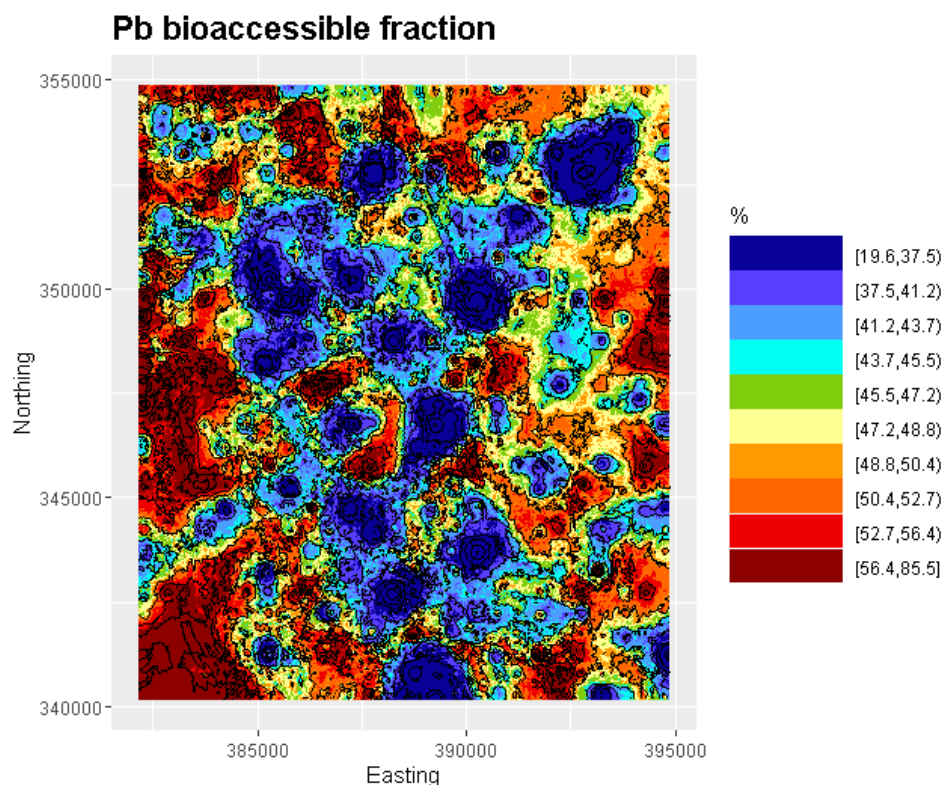


Figure 20. Bioaccessible fraction of Pb in soil in Stoke-on-Trent.

3.3. Relationship with Industry

The Coal Measures, which underlie the city, are naturally elevated in many PHE such as As, V, Mo, Cu, Ni, Zn, Pb [8]. The high concentrations of Pb in particular areas are a likely result of its use as a key constituent in pottery making. English earthenware pottery in the 18th century typically contained PbO (50%wt) compared to 30% in the medieval era [39]. Lead was a key constituent of pottery glazes, acting as a flux, as it was easily and cheaply obtained, had a wide firing temperature range [40], gave good even coverage without fingerprints, prevented crazing and produced brilliant white colour [41]. Lead is also often used in steel production to improve machinability [42]. The steel workings across Stoke-on-Trent and the subsequent use of waste materials for infill material are potential contributors to the dispersal of Pb across the area (Figure 19).

Compared to the distribution pattern of Pb the maps of total and bioaccessible As are more diffuse in nature, reflecting the natural background concentrations associated with the underlying coal measures [43]. High concentrations of total As (>35 mg/kg) were found in Longton near a brick and pipe works and in the surrounding area, in Tunstall and around the Chatterley Whitfield coal workings (Figure 14). Sites with bioaccessible As concentrations greater than 7.4 mg/kg were dotted across the area. In particular, high concentrations were seen at locations of gas and Al works, tile works, brick works and potteries. However, the bioaccessible concentrations were significantly lower than the total concentrations.

The pattern of PHE distribution along the railway lines (WCML, NSR, potteries loop line) served to highlight the association of the presence of Pb in surface soil with the transport of materials to and from industrial activities, e.g., coal, metal production and pottery. Figures 14 and 19 show the close proximity of a range of industrial activities across Stoke-on-Trent. Sites of previous pottery making were often co-located with gasworks, foundries, tileworks and brickworks sites. For example, in Etruria, the potteries were closely associated with a foundry; in Hanley, with a colliery and a foundry and, in Middleport, a pottery and brick/tileworks.

The Stoke-on-Trent Brownfield register for 2021 [44] showed a large number of sites on or close to sites with high concentrations of both total and bioaccessible Pb, primarily near pottery locations, in the east of Etruria and north east of Longport.

4. Conclusions

A combination of laboratory-based bioaccessibility testing, understanding contaminants' chemical forms and spatial geochemistry (with land use information) was used to highlight the impact of historical land use and industrial activities on human exposure to PHE in cities. The bioaccessibility maps represent an important resource for contaminated land risk assessments and land use planning and could be applied as a standard approach for urban centres. Inclusion of predictive bioaccessible fraction mapping provides an indication of the relative mobility of PHE compared to the total PHE concentrations on a wider spatial scale.

This study examined how the combination of RF with IDW predictors could be used to produce spatial prediction models of the total and bioaccessible fractions of potentially harmful elements in an urban environment with quantitative assessment of accuracy and precision. For the purposes of risk assessment, however, the outcomes of the models—namely, the predicted bioaccessible and bioaccessible fractions of As and Pb and their associated uncertainty—were the key measurements arising from the study. These data can be directly used in risk assessment models.

The lack of mineral deposits of Pb and As in the area suggested that the surface contamination was a result of industrial activity. The distribution of As and Pb was most likely driven by industrial activity across Stoke-on-Trent, which is interlinked through transport routes, some of which were specific to particular industries and the linkages between them (e.g., the potteries loop lines, minerals railways and canals). Widespread distribution can be attributed to the plethora of mining activities across the region.

Author Contributions: Conceptualization, methodology, formal analysis, writing—original draft preparation, writing—review and editing J.W. and M.C.; software, M.C. All authors have read and agreed to the published version of the manuscript.

Funding: This research received no external funding.

Data Availability Statement: Total element data from the GSUE sampling programme are available as part of the UK Open Government License.

Acknowledgments: This paper is published with the permission of the Director of the British Geological Survey (Natural Environment Research Council). The contribution of all BGS staff involved in the collection and analysis of samples from the G-BASE survey is gratefully acknowledged. The authors would like to thank the BGS geochemistry laboratories for preparing and analyzing the samples and Antonio Ferreira for his internal review and suggested edits.

Conflicts of Interest: The authors declare no conflict of interest.

References

1. Cave, M.R.; Wragg, J.; Dentys, S.; Jondreville, C.; Feidt, C. Oral Bioavailability. In *Dealing with Contaminated Sites, from Theory towards Practical Application*; Springer: Berlin/Heidelberg, Germany, 2011; pp. 287–324.
2. Cave, M.; Wragg, J. Application of Bioavailability Measurements in Medical Geology. In *Practicalities of Medical Geology*; Springer: Berlin/Heidelberg, Germany, 2021; pp. 235–262.
3. Office for National Statistics. Estimates of the population for the UK, England and Wales, Scotland and Northern Ireland. Available online: <https://www.ons.gov.uk/peoplepopulationandcommunity/populationandmigration/populationestimates/datasets/populationestimatesforukenglandandwalesscotlandandnorthernireland> (accessed on 24 January 2021).
4. Barker, D. The industrialization of the Staffordshire potteries. In *The Archaeology of Industrialization*; Routledge: London, UK, 2020; pp. 203–221.
5. Henrywood, R.K. *Staffordshire Potters, 1781–1900: A Comprehensive List Assembled from Contemporary Directories with Selected Marks*; Antique Collectors' Club: Woodbridge, Suffolk, UK, 2002.
6. MacCarthy, F.; Tisdale, R.; Ayers, W. Geological controls on coalbed prospectivity in part of the North Staffordshire Coalfield, UK. *Geol. Soc. Lond. Spec. Publ.* **1996**, *109*, 27–42. [[CrossRef](#)]

7. Wilson, A.; Rees, J.; Crofts, R.; Howard, A.; Buchanan, J.; Waine, P. Stoke-on-Trent: A Geological Background for Planning and Development. 1992. Available online: <http://nora.nerc.ac.uk> (accessed on 13 May 2021).
8. Fordyce, F.; Ander, E. Urban Soils Geochemistry and GIS-Aided Interpretation: A Case Study from Stoke-on-Trent. 2003. Available online: <http://nora.nerc.ac.uk/id/eprint/7018/> (accessed on 13 May 2021).
9. Chapman, N. *The South Staffordshire Coalfield*; The History Press: Gloucester, UK, 2005.
10. Baker, A.D. *The Potteries Loop Line*; Trent Valley Publications: Manchester, UK, 1986.
11. Gidlow, C.; Ellis, N.; Smith, G.; Fairburn, J. Promoting Green Space in Stoke-on-Trent (ProGreSS). *Young Child.* **2010**, *4*, 113.
12. Scrucca, L.; Fop, M.; Murphy, T.B.; Raftery, A.E. Mclust 5: Clustering, classification and density estimation using Gaussian finite mixture models. *R J.* **2016**, *8*, 289. [[CrossRef](#)] [[PubMed](#)]
13. R Core Team. *R: A Language and Environment for Statistical Computing*; Foundation for Statistical Computing: Vienna, Austria, 2020.
14. Denys, S.; Caboche, J.; Tack, K.; Rychen, G.; Wragg, J.; Cave, M.; Jondreville, C.; Feidt, C. In Vivo Validation of the Unified BARGE Method to Assess the Bioaccessibility of Arsenic, Antimony, Cadmium, and Lead in Soils. *Environ. Sci. Technol.* **2012**, *46*, 6252–6260. [[CrossRef](#)]
15. Wragg, J.; Cave, M.; Basta, N.; Brandon, E.; Casteel, S.; Denys, S.; Gron, C.; Oomen, A.; Reimer, K.; Tack, K.; et al. An inter-laboratory trial of the unified BARGE bioaccessibility method for arsenic, cadmium and lead in soil. *Sci. Total. Environ.* **2011**, *409*, 4016–4030. [[CrossRef](#)]
16. Middleton, D.R.; Watts, M.J.; Beriro, D.J.; Hamilton, E.M.; Leonardi, G.S.; Fletcher, T.; Close, R.M.; Polya, D.A. Arsenic in residential soil and household dust in Cornwall, south west England: Potential human exposure and the influence of historical mining. *Environ. Sci. Process. Impacts* **2017**, *19*, 517–527. [[CrossRef](#)]
17. Watts, M.J.; Button, M.; Brewer, T.S.; Jenkin, G.R.; Harrington, C.F. Quantitative arsenic speciation in two species of earthworms from a former mine site. *J. Environ. Monit.* **2008**, *10*, 753–759. [[CrossRef](#)] [[PubMed](#)]
18. Wragg, J. *BGS Guidance Material 102, Ironstone Soil, Certificate of Analysis*; IR/09/006; British Geological Survey: Keyworth, Nottingham, UK, 2009.
19. Hamilton, E.M.; Barlow, T.S.; Gowing, C.J.; Watts, M.J. Bioaccessibility performance data for fifty-seven elements in guidance material BGS 102. *Microchem. J.* **2015**, *123*, 131–138. [[CrossRef](#)]
20. Wright, M.N.; Ziegler, A. Ranger: A fast implementation of random forests for high dimensional data in C++ and R. *J. Stat. Softw.* **2017**, *77*, 1–17. [[CrossRef](#)]
21. Kursa, M.B.; Rudnicki, W.R. Feature selection with the Boruta package. *J. Stat. Softw.* **2010**, *36*, 1–13. [[CrossRef](#)]
22. Minasny, B.; McBratney, A.B. Spatial prediction of soil properties using EBLUP with the Matérn covariance function. *Geoderma* **2007**, *140*, 324–336. [[CrossRef](#)]
23. Zhu, Q.; Lin, H.S. Comparing Ordinary Kriging and Regression Kriging for Soil Properties in Contrasting Landscapes. *Pedosphere* **2010**, *20*, 594–606. [[CrossRef](#)]
24. Hengl, T.; Nussbaum, M.; Wright, M.N.; Heuvelink, G.B.; Gräler, B. Random forest as a generic framework for predictive modeling of spatial and spatio-temporal variables. *PeerJ* **2018**, *6*, e5518. [[CrossRef](#)]
25. Kirkwood, C.; Cave, M.; Beamish, D.; Grebby, S.; Ferreira, A. A machine learning approach to geochemical mapping. *J. Geochem. Explor.* **2016**, *167*, 49–61. [[CrossRef](#)]
26. Sekulić, A.; Kilibarda, M.; Heuvelink, G.; Nikolić, M.; Bajat, B. Random Forest Spatial Interpolation. *Remote Sens.* **2020**, *12*, 1687. [[CrossRef](#)]
27. Cave, M. A Machine Learning Approach to Geostatistics Applied to Contaminants in Soil 6D.2. In Proceedings of the 7th International Contaminated Site Remediation Conference incorporating the 1st International PFAS Conference, Melbourne, Australia, 10–14 September 2017; pp. 330–331.
28. Vane, C.H.; Kim, A.W.; Beriro, D.; Cave, M.R.; Lopes Dos Santos, R.A.; Ferreira, A.M.; Collins, C.; Lowe, S.R.; Nathanail, C.P.; Moss-Hayes, V. Persistent Organic Pollutants in Urban Soils of Central London, England, UK. 2021. Measurement and Spatial Modelling of Black Carbon (BC), Petroleum Hydrocarbons (TPH), Polycyclic Aromatic Hydrocarbons (PAH) and Polychlorinated Biphenyls (PCB). *Adv. Environ. Eng. Res.* **2021**, *2*, 42. [[CrossRef](#)]
29. Fortin, M.-J.; Dale, M. *Spatial Analysis: A Guide for Ecologists*; Cambridge University Press: Cambridge, UK, 2006.
30. Rawlins, B.; McGrath, S.; Scheib, A.; Breward, N.; Cave, M.; Lister, T.; Ingham, M.; Gowing, C.; Carter, S. *The Advanced Soil Geochemical Atlas of England and Wales*; British Geological Survey: Nottingham, England, UK, 2012.
31. Pebesma, E. sf: Simple Features for R. *R J.* **2018**, *10*, 439–446. [[CrossRef](#)]
32. Team, Q.D. *QGIS Geographic Information System*; Open Source Geospatial Foundation Project, 2021. Available online: <https://www.qgis.org/en/site/about/index.html> (accessed on 12 January 2021).
33. Jenkins, A. *A History of the County of Stafford: Volume 8. Edited by J G Jenkins. Gives a Detailed Account of the History of Newcastle-Under-Lyme and Stoke-on-Trent*; Victoria County History: London, UK, 1963.
34. Biecek, P. DALEX: Explainers for complex predictive models in R. *J. Mach. Learn. Res.* **2018**, *19*, 3245–3249.
35. Cave, M.R.; Wragg, J.; Harrison, H. Measurement modelling and mapping of arsenic bioaccessibility in Northampton, UK. *J. Environ. Sci. Health Part A* **2013**, *48*, 629–640. [[CrossRef](#)] [[PubMed](#)]
36. Appleton, J.; Cave, M.; Wragg, J. Modelling lead bioaccessibility in urban topsoils based on data from Glasgow, London, Northampton and Swansea, UK. *Environ. Pollut.* **2012**, *171*, 265–272. [[CrossRef](#)] [[PubMed](#)]
37. Anheuser, K. The practice and characterization of historic fire gilding techniques. *JOM* **1997**, *49*, 58–62. [[CrossRef](#)]

38. Hunt, L.B. Gold in the pottery industry. *Gold Bull.* **1979**, *12*, 116–127. [CrossRef]
39. Tite, M.; Freestone, I.; Mason, R.; Molera, J.; Vendrell-Saz, M.; Wood, N. Lead glazes in antiquity—Methods of production and reasons for use. *Archaeometry* **1998**, *40*, 241–260. [CrossRef]
40. This Day in Pottery History. Available online: <https://thisdayinpotteryhistory.wordpress.com/category/pottery-types/lead-glaze/> (accessed on 18 June 2021).
41. Staffordshire County Council. Staffordshire Past Track. Available online: <https://www.search.staffspasttrack.org.uk/Details.aspx?&ResourceID=15195&PageIndex=8&SearchType=2&ThemeID=515> (accessed on 18 June 2021).
42. Lead in Steel. Available online: <https://www.ispatguru.com/lead-in-steels/#:~:text=Influence%20of%20lead%20on%20steels,and%20permitting%20increased%20machine%20speed> (accessed on 18 June 2021).
43. Appleton, J.D.; Cave, M.R.; Wragg, J. Anthropogenic and geogenic impacts on arsenic bioaccessibility in UK topsoils. *Sci. Total. Environ.* **2012**, *435–436*, 21–29. [CrossRef]
44. Stoke-on Trent Brownfield Register. Available online: <https://data.gov.uk/dataset/1368fc6f-3975-4bf1-b234-1f5d6055b7dd/stoke-on-trent-brownfield-register> (accessed on 12 January 2021).